

Improvement of Electrochemical Capability of Sputtered Silicon Film Anode for Rechargeable Lithium Batteries

Shinichi Komaba,*† Fuminobu Mikami, Tatsuya Itabashi, Mamoru Baba, Taku Ueno, and Naoaki Kumagai

Department of Frontier Materials and Functional Engineering, Graduate School of Engineering, Iwate University, 4-3-5 Ueda, Morioka 020-8551

Received March 25, 2005; E-mail: komaba@rs.kagu.tus.ac.jp

To improve the electrochemical properties of the silicon film anode in lithium cells, we prepared three types of silicon based-films, i.e., intrinsic silicon, n-type silicon, and $Ag_{10}Si_{90}$ binary films using r.f. magnetron sputtering. Based on galvanostatic charge–discharge tests and a.c. impedance measurements, the n-type silicon film and $Ag_{10}Si_{90}$ binary film cells exhibited a superior cycle life and lower electrochemical resistance compared with the intrinsic silicon film cell. The potential variation in the electrochemical alloying/de-alloying reactions of the $Ag_{10}Si_{90}$ binary film with lithium was different from that of the intrinsic silicon film, meaning that the Ag ingredient in the binary film affected the charge–discharge reaction. Furthermore, when a Ni plate roughened by chemical etching was used as a substrate, the $Ag_{10}Si_{90}$ film anode demonstrated an excellent capacity retention during 400 cycles with a high discharge capacity of $>200\,\mu A\,h\,cm^{-2}$ (corresponding to $1500\,mA\,h\,g^{-1}$) at $0.5\,mA\,cm^{-2}$ (2.5 C).

In recent times, crystalline carbonaceous materials have been used as a commercial lithium-ion battery anode whose theoretical capacities are approximately $372\,mA\,h\,g^{-1}$. In order to increase the energy density of the lithium-ion battery, many researchers have studied alternative anode materials. A silicon electrode material is one of the best candidates for the alternative anodes, since silicon is known to form lithium alloys, such as $Li_{1.31}Si$, $Li_{2.33}Si$, $Li_{3.25}Si$, and $Li_{4.4}Si$ phases. When these Li–Si alloys are electrochemically formed, the theoretical capacity is approximately $4200\,mA\,h\,g^{-1}$, much higher than that of the carbonaceous materials.[1,2] However, the silicon anode suffers from a large volume change during charge–discharge leading to cracking and pulverization of the silicon particles,[3] which result in drastic capacity fading. In previous reports to solve this problem, a nano-silicon composite material was prepared by mixing nano-size silicon powder and carbon black.[4] Yoshio et al. reported that the high capacity performance of carbon-coated silicon was prepared by the thermal vapor decomposition method.[5] To control the reversible capacity, a nanocomposite of inactive material (TiN and TiB_2) and silicon was prepared by mechanical milling.[6,7] Several silicides with several metals (i.e. Fe, Mg, Ni, and Ca) and their composite with graphite were prepared by a mechanical alloying (MA) method.[8–11]

Recently, silicon thin films have also been investigated as an anode for lithium-ion batteries. The amorphous silicon film possessed a high discharge capacity which corresponds to almost the theoretical capacity by controlling the thickness of the silicon film.[12,13] Furthermore, the silicon film exhibited an excellent charge–discharge cycling behavior at a high current density as described by Takamura and co-workers.[14] The metal–silicon alloy films were prepared by co-depositing with metal and silicon sources, for example, a Si–Zr alloy thin film showed an improved electrochemical performance by controlling the distribution of the inactive zirconium element in the films.[15] Beaulieu et al. studied the volume change of the Si–Sn alloy film during the charge–discharge reaction by in-situ atomic force microscopy,[16] proving that the volume expansion coefficient of the Si–Sn alloy film was 250% lower than that of the silicon film (300%).

In this paper, we prepared intrinsic silicon, n-type silicon, and $Ag_{10}Si_{90}$ binary film electrodes by r.f. magnetron sputtering to clarify the difference in the electrochemical behavior and the relationship between the electric conductivity and electrochemical performance. Furthermore, the films were deposited on a roughened substrate to improve the cycle life by suppressing the pulverization and stress.

Experimental

Silicon films were deposited on flat Ni substrates (Nilaco Co.) by r.f. magnetron sputtering. The pressure of the sputtering chamber reached approximately 1×10^{-5} Torr using a vacuum turbopump. The size of the intrinsic silicon target (Furuuchi Chemical Co., 99.999% purity, (100) orientation) and phosphorus-doped n-type silicon(100) wafer (Komatsu Electric Metal Co., specific resistance: 0.036–0.037 Ω cm, dopant concentration: about 1.40×10^{17} atoms cm^{-3}) was 80 mm in diameter. The sputtering conditions were as follows: Pressure inside the chamber was maintained at 1×10^{-2} Torr by flowing argon gas during deposition, and the r.f. power was kept at 80 W. The $Ag_{10}Si_{90}$ film was similarly deposited by putting a silver pellet (13 mm in diameter) made of compressed silver powder (Aldrich, 99.9% purity) on the intrinsic silicon target. The thickness of their films was adjusted to approximately 0.6 μm as determined by the roughness measuring instru-

† Present address: Department of Applied Chemistry, Tokyo University of Science, 1-3 Kagurazaka, Shinjuku-ku, Tokyo 162-8601

Published on the web January 13, 2006; DOI 10.1246/bcsj.79.154

ment (Tylor Hobson, Ltd., Form Talysurf Series 2). For comparison, an Ag film was deposited on a Ni substrate by vacuum evaporation, to a thickness of 0.2 μm.

The flat nickel substrate was roughened by chemical etching in a 1 mol dm^{-3} iron(III) chloride aqueous solution for 90 s at room temperature prior to the sputtering. The silicon film electrodes with an area of 1.0 × 1.0 cm^2 were formed on the nickel substrate using a stainless mask.

The electrochemical performance of the film electrodes in lithium cells was investigated with a three-electrode cell using lithium foils as counter and reference electrodes and the silicon films as a working electrode. The electrolyte used was 1 mol dm^{-3} $LiClO_4$ in a 1:1 v/v mixture of ethylene carbonate (EC) and diethyl carbonate (DEC). The cells were assembled in an argon-filled glove box. Galvanostatic charge–discharge tests were carried out between 0.02 and 1.5 V vs Li/Li$^+$ at 0.5 mA cm^{-2} in the glove box. Cyclic voltammetry was performed by sweeping the potential at the rate of 0.05 mV s^{-1}. Alternate current impedance measurements were carried out in the frequency range from 100 kHz to 10 mHz with a perturbation voltage of 3 mV.

X-ray diffraction (Rigaku, RINT2200) was employed for the analysis of the thin films. The surface morphology of an electrode (before and after charge–discharge tests) and distribution of the silver ingredient in the $Ag_{10}Si_{90}$ alloy film were observed by scanning electron microscopy (SEM) (Hitachi, N-2250NII) along with an energy dispersive X-ray analysis (Hitachi, N-2300NII).

Results and Discussion

n-Type Silicon Film. As previously reported, the n- or p-type silicon film was prepared by a sputtering method with the corresponding wafers.[17–19] In this study, a silicon film was also prepared by r.f. magnetron sputtering of an n-type silicon wafer (0.036–0.037 Ω cm) as the target. Therefore, we believe that the silicon film obtained by the sputtering was an n-type semiconductor, and the electrochemical property of the silicon films was dramatically changed by a tiny amount of phosphorus dopant as mentioned below.

In order to investigate the crystalline state of the silicon films deposited by the sputtering, the XRD patterns of the intrinsic silicon film is shown in Fig. 1. The three intense Ni peaks in the pattern are due to the substrate. An additional two peaks around 40 and 47° in the XRD pattern are attributed to the (111) and (200) of the crystalline silicon, respectively. Therefore, we suggest that the sputtered film consisted of almost crystalline cubic silicon. The XRD pattern of the n-type silicon was also the same as that of the intrinsic film in Fig. 1, supporting the fact that the phosphorus dopant (about 1.4 × 10^{17} atoms cm^{-3}) has almost no influence on the crystallinity of the resultant silicon thin film.

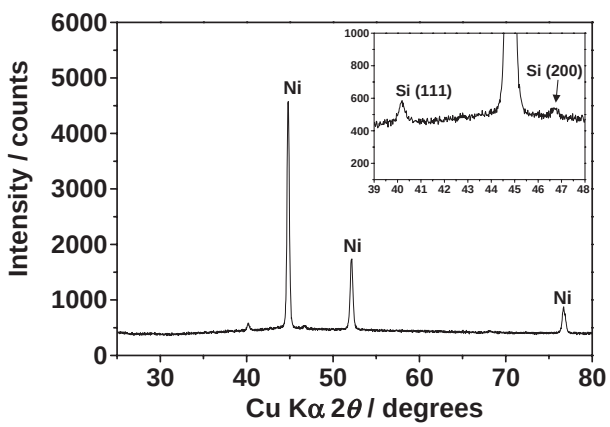

Fig. 1. XRD patterns of intrinsic Si thin film with thickness of 0.6 μm formed on Ni substrates by r.f. magnetron sputtering.

The galvanostatic charge–discharge curves of the intrinsic and the n-type silicon film electrodes for the first and second cycles are shown in Fig. 2. The two silicon films obviously indicated a charge–discharge performance due to the electrochemical activity of the reversible Li$^+$ alloying/de-alloying. The charge (electro-reduction) reaction mainly occurred below 0.3 V, and the discharge (electro-oxidation) capacity appeared from 0.2 to 0.8 V for both silicon films. The first discharge capacities of the intrinsic silicon film and n-type silicon film were 316.8 and 265.6 μA h cm^{-2} (corresponding to 2266 and 1900 mA h g^{-1}, respectively, which were estimated by assuming a crystalline silicon density is 2.33 g cm^{-3}). It is clear that the first and second discharge capacities of the intrinsic silicon film are greater than those of the n-type silicon film. It is probable that the n-type doping influenced the electrochemical nature of the silicon films. We observed that the irreversible capacity of both silicon films appears during the first and second cycles. This suggests that the crystal structure of the silicon films could gradually become amorphous during the initial several cycles accompanied by a rearrangement of the Si–Si bonding, so that the irreversible capacities occurred due to entrapment of a definite amount of lithium in the rearranged silicon matrix.

In the magnified profile of the first charge curve, however, polarization during the first lithiation of the n-type silicon film is smaller than that of the intrinsic silicon film around 0.3 V. Moreover, the "potential overshoot" around 0.25 V appears during the initial charge stage of the intrinsic silicon film, but it hardly appears for the n-type silicon film. Huggins et al. reported that the potential overshoot occurs due to the existence of a nucleation barrier in the first process of the Li–Si

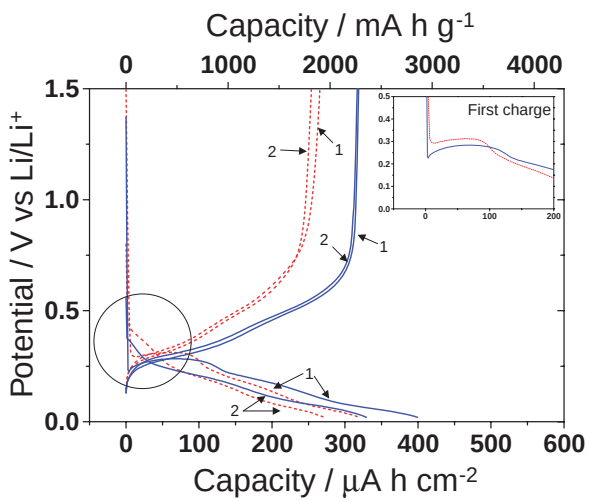

Fig. 2. Galvanostatic charge–discharge curves at the first and second cycles of intrinsic Si film (solid line) and n-type Si film electrodes (dashed line) whose thickness was 0.6 μm at 0.5 mA cm^{-2}.

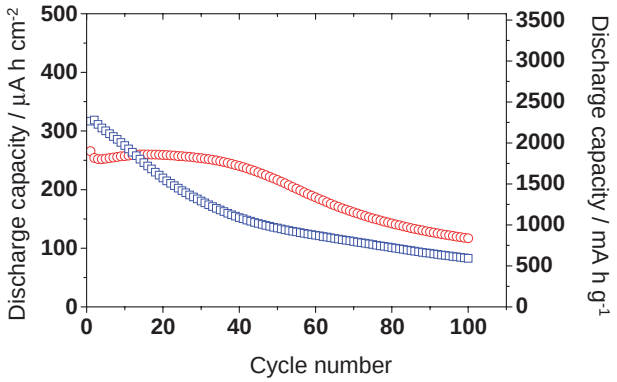

Fig. 3. Discharge capacity vs cycle number plots obtained from galvanostatic charge–discharge tests of intrinsic Si film (□) and n-type Si film (○) electrodes (thickness: 0.6 μm) at 0.5 mA cm^{-2}.

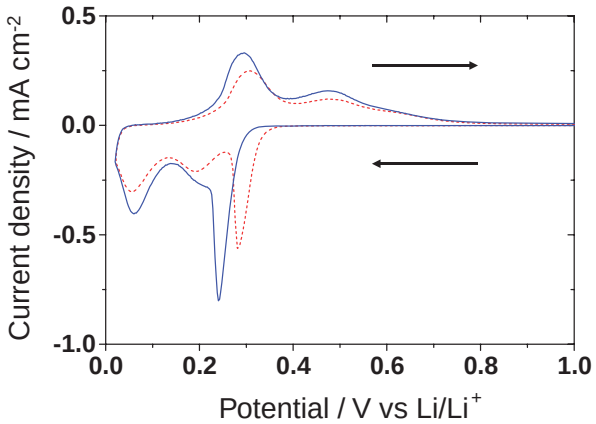

Fig. 4. Cyclic voltammograms of intrinsic Si (solid line) and n-type Si (dashed line) film electrodes (thickness: 0.6 μm) at 0.05 mV s^{-1}.

phase formation, and it disappears in the second charge curve.[2] It is thought that the same overshoot is observed for these silicon films formed by sputtering. From these results, we found that: (i) The polarization during the first lithiation of the n-type silicon film is smaller than that of the intrinsic silicon film, and (ii) the potential overshoot hardly occurred during the first charge for the n-type silicon film. It is likely that this difference was due to the enhancement of the electric conductivity of the silicon film by the phosphorus doping and by the nucleation barrier of the Li–Si alloy formation.[2]

The discharge capacity vs cycle number plots of the intrinsic and n-type silicon films are shown in Fig. 3. For the intrinsic silicon film, its discharge capacities gradually faded to 82.9 μA h cm^{-2} (corresponding to 592.3 mA h g^{-1}) after 100 cycles. In contrast, the discharge capacity of the n-type silicon film was maintained at over 200 μA h cm^{-2} (corresponding to 1500 mA h g^{-1}) until about 50 cycles. This suggests that the n-type silicon film maintained its electrochemical activity by increasing the electric conductivity in the film, although the intrinsic silicon film having the lower conductivity deteriorated due to cracking and pulverization during the charge–discharge cycling. Moreover, the discharge capacity of the n-type silicon film gradually increased for about 20 cycles. It is likely that this phenomenon occurred due to the influence of the phosphorus present in the n-type silicon film.

To investigate the electrochemical redox behavior of the silicon film electrodes, cyclic voltammetry was carried out as shown in Fig. 4. There appear three redox couples in both voltammograms of the intrinsic and the n-type silicon films. These peaks were attributed to the lithium alloy formation with silicon.[20] However, the first reduction of the n-type silicon film is observed at the higher potential than that of the intrinsic silicon film. This is coincident with the lower polarization during the first lithiation of the n-type silicon film than that of the intrinsic silicon film around 0.3 V as seen in Fig. 2. Consequently, the inclusion of phosphorus in the silicon film was effective for improving the anode performance.

In order to discuss the electrode impedance during the alloying reaction of silicon, a.c. impedance measurements were performed during the first cycle of the two silicon films as shown in Fig. 5. Two semicircles appeared in all the Cole–Cole plots. As similar semicircles were observed in the case of the carbonaceous anodes,[21] we considered the first semicircle in the higher frequency region and the second semicircle in the middle frequency region to be due to the electrolyte/electrode interface resistance including the surface passivation layer and the silicon bulk resistance, respectively. Whereas the first and second semicircles of both silicon films hardly change during the charge reaction (Figs. 5a and 5b), the second semicircles drastically increase at the same potential. This suggests that the cracking and pulverization of the silicon particles occur with a huge volume change, resulting in the increased resistance of both silicon electrodes. Moreover, the first semicircle of both Cole–Cole plots barely increases at 0.6 V during the discharge (Fig. 5d). It is probable that the reductive decomposition occurs much severely at the new silicon surface formed by the cracking and pulverization, resulting in the higher resistive deposits at the electrolyte/electrode interface during the end of the discharge reaction.

Furthermore, the semicircles of the n-type silicon film are confirmed to be always smaller than those of the intrinsic silicon film. It is suggested that the enhancement of the electrochemical activity of the n-type silicon film is due to the lower resistance of both semicircle components. In addition, the bulk resistance of the n-type silicon film must be lower than that of the intrinsic silicon film. The improved maintenance of the electric contact within the silicon film during cycling would be achieved by the higher electric conductivity and the phosphorus ingredient of the n-type silicon film, although the intrinsic or pure silicon film was severely affected by cracking and pulverization.

These results confirm that the electrochemical performance of the n-type silicon film electrode in lithium cells is superior to that of the undoped silicon film, that is, the electric conductivity and doping of the silicon film are the important factors for enhancing the reversible reaction of the Si–Li alloy.

$Ag_{10}Si_{90}$ Binary Film. In the previous report on the graphite anode, the battery performance was improved by silver particles dispersed in the graphite electrode.[22] To investigate the effect of silver in the silicon film and compare it to the silicon film, we prepared the $Ag_{10}Si_{90}$ film by the co-sputtering method with a target consisting of both the intrinsic silicon wafer

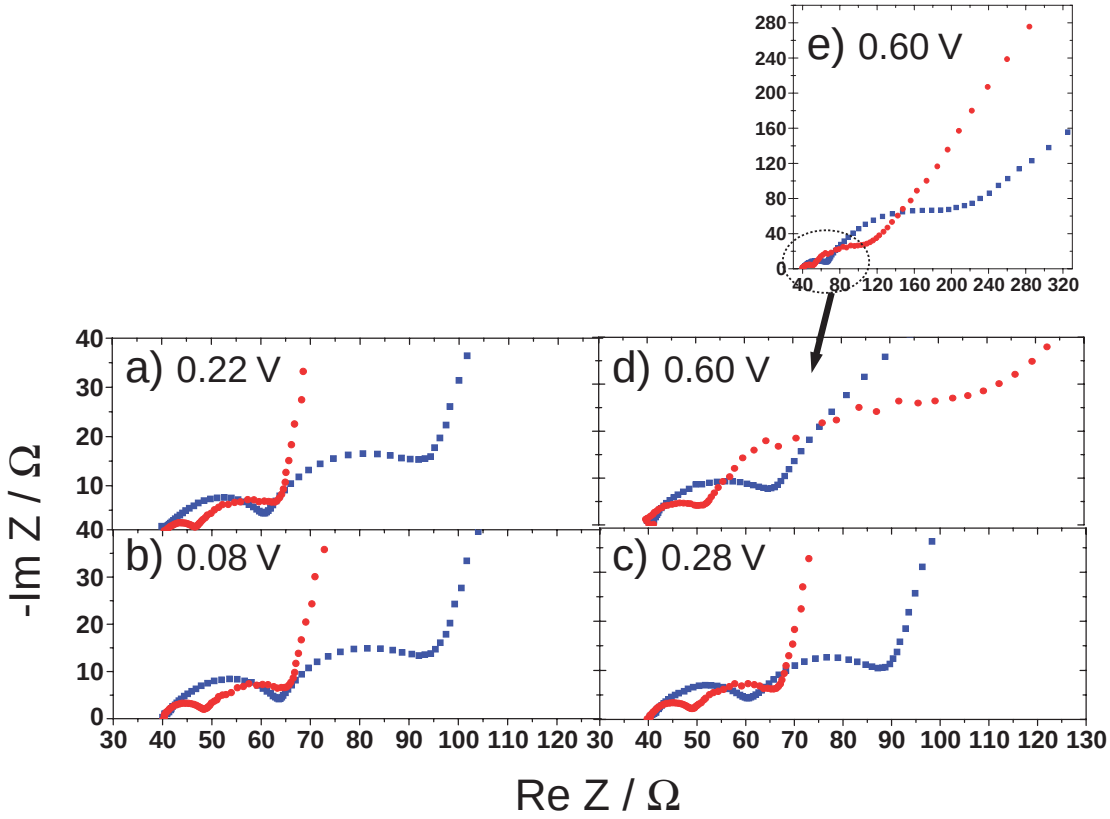

Fig. 5. Cole–Cole plots of intrinsic Si (■) and n-type Si (●) film electrodes measured during galvanostatic the first cycle at a) 0.22 V and b) 0.08 V of the charge, c) 0.28 V, and d), e) 0.60 V of the discharge.

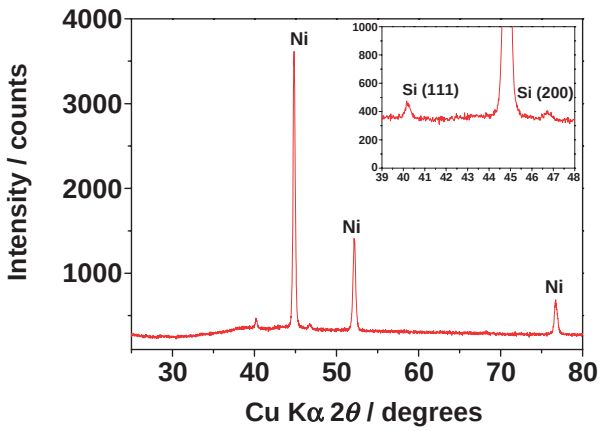

Fig. 6. XRD patterns of $Ag_{10}Si_{90}$ thin films with thickness of 0.6 μm formed on Ni substrates by r.f. magnetron sputtering.

and a silver pellet. The chemical composition of the resultant film was adjusted by controlling the ratios of the surface area and the shape of the Ag pellet on the silicon wafer, as confirmed by X-ray photoelectron spectroscopy (XPS).

Figure 6 shows the XRD patterns of the $Ag_{10}Si_{90}$ film. Ni peaks in the XRD pattern come from the substrate. Two small peaks around $2\theta = 40$ and 47° are attributed to crystalline silicon as well as the intrinsic silicon film as seen in Fig. 1. Therefore, the $Ag_{10}Si_{90}$ binary film deposited by sputtering also mainly consisted of crystalline cubic silicon, while no peak attributed to crystalline silver was observed. Therefore, we carried out SEM-EDX measurements to investigate the existence and distribution of the silver component in the binary film.

The SEM image and corresponding EDX elemental maps are shown in Fig. 7. The $Ag_{10}Si_{90}$ binary film was partly peeled off the Ni substrate by intentionally scratching the film surface prior to observation. In Fig. 7, one can see the flat morphology of a piece of the scratched silicon film. It is clear that the scratched film consisted of silicon and silver, and they are uniformly dispersed in the entire film on a sub-micron scale. Since the silver ingredient exists in the film and no diffraction peak of metallic silver appeared in Fig. 6, an amorphous Ag–Si alloy phase or amorphous silver could be contained in the film, most likely as a nanocomposite of silver and silicon that was formed under this sputtering conditions.

The galvanostatic charge–discharge curves for the first and second cycles of the $Ag_{10}Si_{90}$ binary film are shown in Fig. 8, and compared to those of the intrinsic silicon film. The binary film also exhibited a charge–discharge performance with a high capacity as did the silver-free silicon films. The discharge capacities of the $Ag_{10}Si_{90}$ film, approximately 350 μA h cm^{-2} (corresponding to 2500 mA h g^{-1}), are greater than those of the intrinsic silicon film, whereas lower discharge capacities of the n-type silicon film compared to those of the intrinsic silicon film were obtained during the initial cycles as can be seen in Fig. 3. We believe that the silver influenced the charge–discharge reaction. During the first charge of the $Ag_{10}Si_{90}$ film, a voltage plateau appeared around 0.33 V, which is higher than those of the intrinsic silicon and n-type silicon films. There-

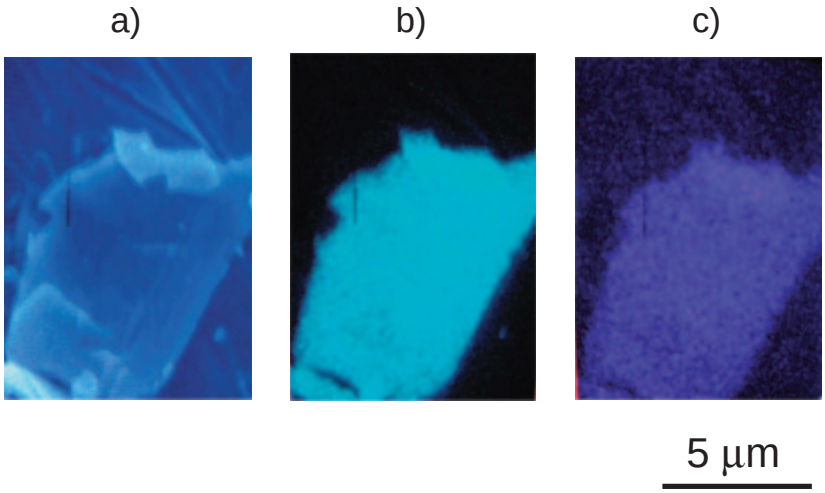

Fig. 7. a) SEM image and corresponding element maps of b) Si and c) Ag of the $Ag_{10}Si_{90}$ film. As an observed morphology, intentionally scratched a film surface.

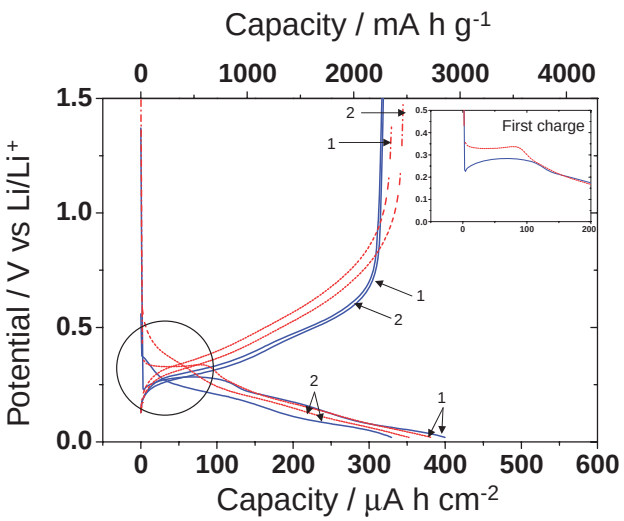

Fig. 8. Galvanostatic charge–discharge curves (0.5 mA cm^{-2}) at the first and second cycles of intrinsic Si (solid line) and $Ag_{10}Si_{90}$ film electrodes (dashed line) with thickness of 0.6 μm.

fore, the polarization of the first lithiation of the $Ag_{10}Si_{90}$ film was reduced in comparison with those of the silicon films. Moreover, the "potential overshoot," which was observed in Fig. 2, hardly appears in the charge curve of the $Ag_{10}Si_{90}$ binary film. These results suggest that the Si–Li alloy nucleation barrier is depressed and the electric conductivity of the silicon film was improved by the silver doping as well as the n-type silicon film.

To observe the details of the electrochemical reaction of the $Ag_{10}Si_{90}$ film during the first cycle, cyclic voltammetry was examined as shown in Fig. 9. For the $Ag_{10}Si_{90}$ binary film, three reductive peaks are distinguishable below 0.4 V, and the first sharp peak, which appeared at about 0.3 V, is due to the electrochemical alloying of silicon with lithium. Because the reductive current for the intrinsic silicon film began to flow at the lower potential around 0.2 V (Fig. 9b), the electrochemical alloying of silicon with Li in the first charge reaction oc-

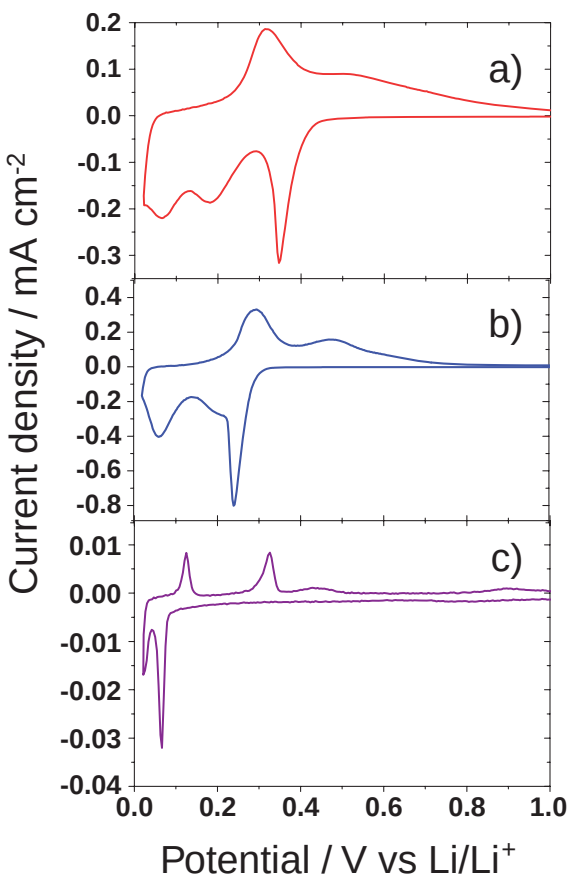

Fig. 9. Variations in cyclic voltammograms of a) $Ag_{10}Si_{90}$ film, b) Si film, and c) Ag film electrodes at 0.05 mV s^{-1}.

curred more readily with the silver dopant similar to the n-type film. Moreover, the $Ag_{10}Si_{90}$ film obviously reacted below 0.05 V with a relatively high reductive current similar to the silver film in the lower potential (<0.1 V) region where the initial Ag–Li alloy formation occurred (Fig. 9c). It is probable that the amorphous silver also participation in the charge–discharge reaction as expected in Figs. 6 and 7.

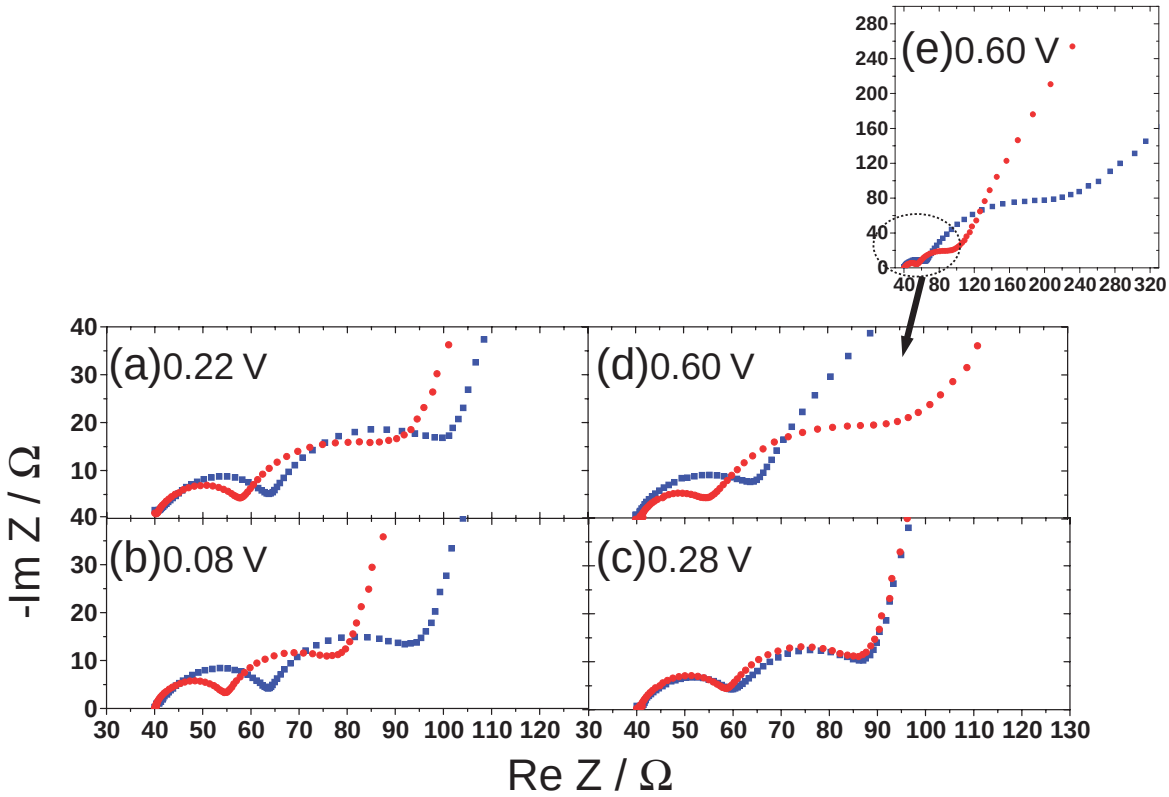

Fig. 10. Cole–Cole plots of Si (■) and $Ag_{10}Si_{90}$ (●) film electrodes measured during galvanostatic the first cycle at a) 0.22 V and b) 0.08 V of the charge, c) 0.28 V, and d), e) 0.60 V of the discharge.

For discussing the electrochemical impedance during the first charge–discharge reaction, the Cole–Cole plots were drawn at the potentials where the reactive peaks were observed in the cyclic voltammogram of Fig. 9. In the Cole–Cole plots for a charge potential at 0.22 V (Fig. 10a), the first semicircles in the higher frequency region can be assumed to be due to the electrolyte/electrode interface as mentioned above.[21] The interface resistance of the $Ag_{10}Si_{90}$ binary film is somewhat lower than that of the intrinsic film. This result is coincident with the smaller polarization at the beginning of the first lithiation of the $Ag_{10}Si_{90}$ alloy film in comparison with the intrinsic silicon film as seen in Fig. 8. Moreover, the two semicircles of the $Ag_{10}Si_{90}$ film at the other potentials are always smaller than those of the intrinsic silicon film. At 0.60 V (Fig. 10d), especially, the second semicircle of the $Ag_{10}Si_{90}$ alloy film, whose diameter was about 65 Ω is extremely smaller than that of the intrinsic silicon film (about 235 Ω). This means that the cracking more severely occurred during the charge–discharge for the intrinsic silicon film, resulting in the partial electrical isolation of the silicon.

The discharge capacity vs cycle number plots of the intrinsic silicon film and $Ag_{10}Si_{90}$ binary film are shown in Fig. 11. The $Ag_{10}Si_{90}$ binary film exhibits an improved cycle life compared to the intrinsic silicon film, that is, 178 μA h cm^{-2} (corresponding to 1275 mA h g^{-1}) was maintained after 100 cycles. As the volume change of the silicon film was reduced by alloying with a heterogeneous metal,[16] the volume change of the $Ag_{10}Si_{90}$ alloy film should be suppressed in comparison with that of the intrinsic silicon film in the first cycle. Namely,

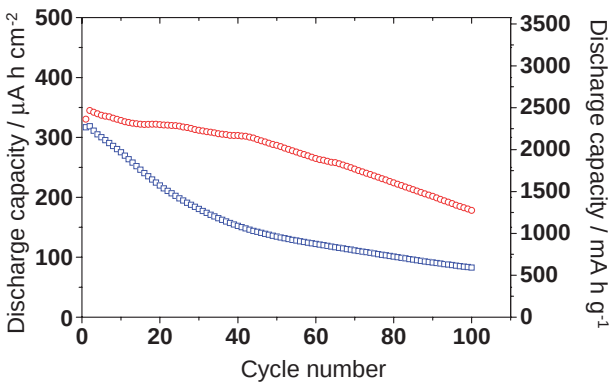

Fig. 11. Discharge capacity vs cycle number plots obtained from galvanostatic charge–discharge tests of Si film (□) and $Ag_{10}Si_{90}$ film (○) electrodes (thickness: 0.6 μm) at 0.5 mA cm^{-2}.

the cracking and pulverization of the silicon film were suppressed so that an improved electrical contact among silicon particles was achieved.

Since the film morphology of the silicon films is dramatically changed by alloying as is generally known, the intrinsic silicon film and the $Ag_{10}Si_{90}$ binary film after cycling are shown in Fig. 12. It was confirmed that the surface morphology of the silicon films was flat and smooth before cycling. From the SEM images, the silicon films were damaged after 100 cycles because of the huge volume change during the charge–discharge reaction. The intrinsic silicon film seemed to become

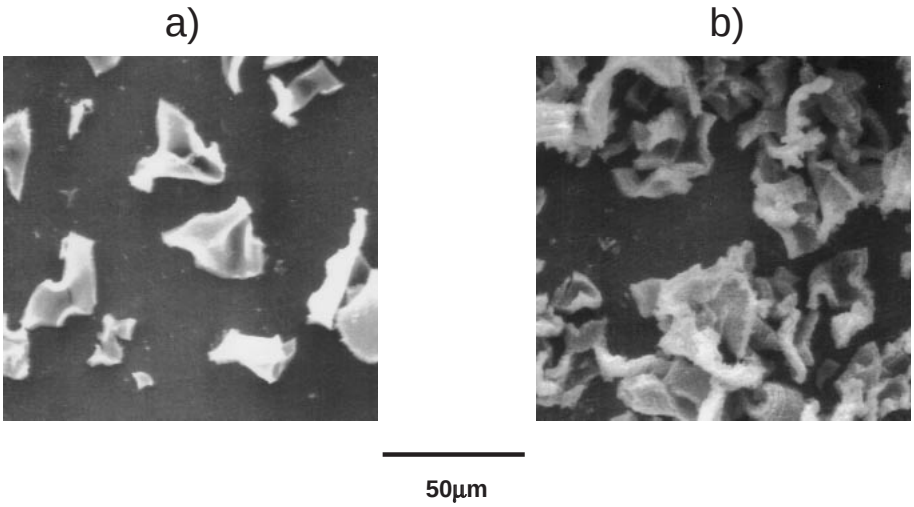

Fig. 12. SEM images of a) Si film and b) $Ag_{10}Si_{90}$ film after 100 cycles.

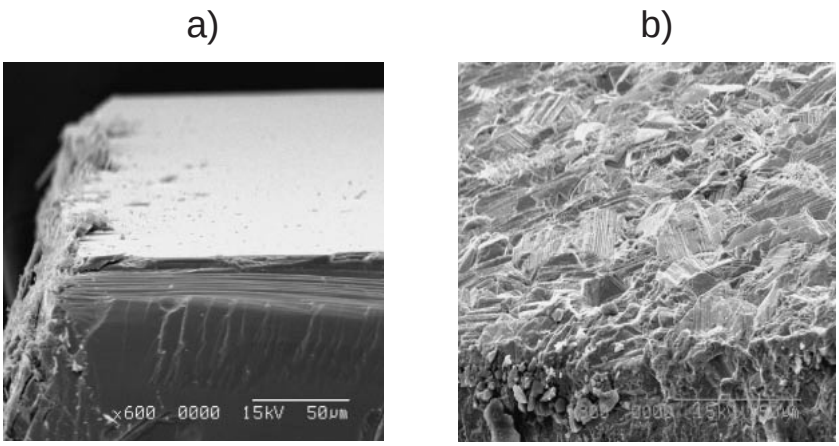

Fig. 13. SEM images of a) pristine Ni and b) etched Ni substrates by dipping a 1 mol dm^{-3} $FeCl_3$ aqueous solution for 90 s at room temperature.

curled pieces on the Ni substrate, whose size was 10–50 μm and each piece was isolated. The morphology of the $Ag_{10}Si_{90}$ film similarly changed, however, the pieces were substantially in contact with each other and possessed an electrical contact with the Ni substrate.

From these results, one can note that the $Ag_{10}Si_{90}$ film exhibited a higher capacity with improved cycle life that is comparable to that of the n-type silicon film. It is thought that the volume change of the film decreased due to the coexistence of silver in the film involved in the charge–discharge reaction, resulting in suppression of the binary film collapse.

Further Improvement by Pretreatment of Ni Substrate. The main problem to achieve a sufficient cycleability is that the silicon films are partly separated and isolated from the Ni substrate due to the volume change, suggesting that the surface condition of the Ni substrate was one of the key factors to determine adhesion of the silicon films to the Ni substrate. To improve the cycle life of the silicon films, the Ni substrate, roughened by chemical wet etching with Fe(III), was employed as a substrate as shown in Fig. 13. Compared to the pristine substrate, the surface was effectively roughened by the oxidation of nickel by trivalent iron ions.

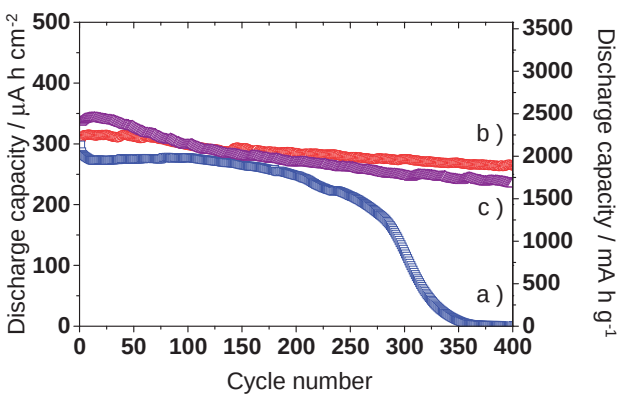

Fig. 14. Variations in discharge capacities at 0.5 mA cm^{-2} of a) Si film, b) $Ag_{10}Si_{90}$ film, and c) n-type Si film on an etched Ni substrate.

The intrinsic silicon, n-type silicon, and $Ag_{10}Si_{90}$ binary films were deposited on the roughened Ni substrates, and the variation in their discharge capacities of the silicon films during 400 cycles are shown in Fig. 14. Compared to the results in

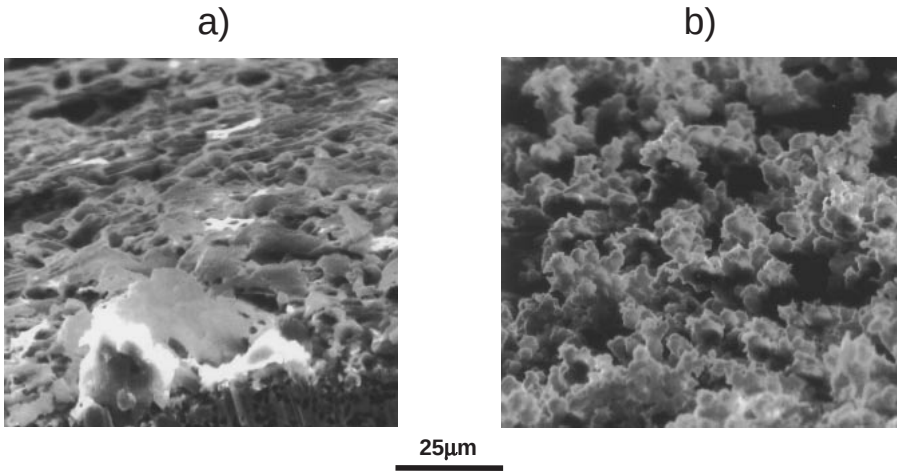

Fig. 15. SEM images of surface of the intrinsic Si film on an etched Ni substrate a) before and b) after galvanostatic charge–discharge cycling of 300 cycles at 0.5 mA cm^{-2}.

Figs. 3 and 11, the adoption of a roughened Ni substrate significantly improves the cycleability of the silicon based thin film anodes. This suggests that the rough surface of a substrate effectively improves the silicon/substrate interface properties, that is, the thickness of the deposited film is not uniform and the mean thickness is expected to be less than 0.6 μm because of the higher surface area of the roughened substrate. The n-type silicon and $Ag_{10}Si_{90}$ binary films demonstrated a satisfactory of cycle life of over 400 cycles with a higher capacity of over 200 μA h cm^{-2} (>1500 mA h g^{-1}), whereas the capacities of the intrinsic silicon film gradually faded after 200 cycles and quickly decreased around the 300th cycle. After 350 cycles, almost no capacity was obtained using the silicon film. From these results, this capacity retention depended on the fatigue of the electrical contact among the silicon particles by the electrochemical volume change, which can be suppressed by roughening the surface of the substrate.

The surface morphologies of the intrinsic silicon film deposited on the roughened substrate before and after 300 cycles are illustrated in Fig. 15. Before cycling, the parent silicon film was also rough and its thickness is heterogeneous as expected. After 300 cycles, the film morphology had degenerated with the electrochemically induced volume change. Also, the morphology is different from that of Fig. 12. In case of the roughened substrate, there appear many small particles which might be deposited by decomposition of the electrolyte solution. Although the discharge capacity of the intrinsic silicon film dramatically faded when over 350 cycles as shown in Fig. 14, the improved electrical contact within the silicon film may be maintained by comparison with the results in Fig. 11.

It was found that the $Ag_{10}Si_{90}$ film on the chemically etched substrate exhibited an excellent cycle life of over 400 cycles with the discharge capacity of about 300 μA h cm^{-2} (corresponding to 2000 mA h g^{-1}) for the thickness of 0.6 μm. This film anode material has potential for application as a high capacity electrode in the lithium-ion battery. Further investigation for higher absolute capacities with thicker silicon films or silicon powders is now in progress based on these fundamental achievements.

Conclusion

We prepared intrinsic silicon, n-type silicon, and $Ag_{10}Si_{90}$ binary film electrodes by r.f. magnetron sputtering and investigated their electrochemical performance. It was found that the electric conductivity and chemical nature of the silicon-based films played a key role in determining their battery performances. The charge–discharge tests confirmed that the polarization of the first lithiation of the n-type silicon and $Ag_{10}Si_{90}$ films was smaller than that of the undoped silicon film, and these films exhibited a sufficient cycle life with a lower barrier for the Si–Li nucleation. Moreover, electrochemical impedances of these films during charge–discharge cycling were lower than that of the intrinsic silicon film. Hence, the n-type silicon and $Ag_{10}Si_{90}$ binary films deposited on the roughened Ni substrates demonstrated a sufficient cycle life of over 400 cycles at greater than 200 μA h cm^{-2} (>1500 mA h g^{-1}).

The authors thank Ms. N. Kumagai, Mr. K. Ohta, Ms. A. Ueyama, and Mr. S. Takahashi for their helpful assistance in the experimental work. This study was financially supported by the program in '00–'04 "*Development of Rechargeable Lithium Battery with High Energy/Power Density for Vehicle Power Sources*" of the Industrial Technology Research Grant Program from the New Energy and Industrial Technology Development Organization (NEDO), Japan.

References

1 R. A. Sharma, R. N. Seefurth, *J. Electrochem. Soc.* **1976**, *123*, 1763.
2 R. A. Huggins, *J. Power Sources* **1996**, *81–82*, 13.
3 M. Winter, J. O. Besenhard, *Electrochim. Acta.* **1999**, *45*, 31.
4 H. Li, X. J. Huang, L. Q. Chen, Z. Wu, Y. Liang, *Electrochem. Solid-State Lett.* **1999**, *2*, 547.
5 M. Yoshio, H. Wang, K. Fukuda, T. Umeno, N. Dimov, Z. Ogumi, *J. Electrochem. Soc.* **2002**, *149*, 1598.
6 I. S. Kim, P. N. Kumta, G. E. Blomgren, *Electrochem.*

Solid-State Lett. **2000**, *3*, 493.
7 I. S. Kim, G. E. Blomgren, P. N. Kumta, *Electrochem. Solid-State Lett.* **2003**, *6*, 157.
8 H.-Y. Lee, S.-M. Lee, *J. Power Sources* **2002**, *112*, 649.
9 G. A. Roberts, E. J. Cairns, J. A. Reimer, *J. Power Sources* **2002**, *110*, 424.
10 G. X. Wang, L. Sun, D. H. Bradhurst, S. Zhong, S. X. Dou, H. K. Liu, *J. Alloys Compd.* **2000**, *306*, 249.
11 J. Wolfenstine, *J. Power Sources* **2003**, *124*, 241.
12 H. Jung, M. Park, Y.-G. Yoon, G.-B. Kim, S.-K. Joo, *J. Power Sources* **2003**, *115*, 346.
13 J. P. Maranchi, A. F. Hepp, P. N. Kumta, *Electrochem. Solid-State Lett.* **2003**, *6*, 198.
14 T. Takamura, S. Ohara, M. Uehara, J. Suzuki, K. Sekine, *J. Power Sources* **2004**, *129*, 96.
15 S.-J. Lee, H.-Y. Lee, H.-K. Baik, S.-M. Lee, *J. Power Sources* **2003**, *119–121*, 113.
16 L. Y. Beaulieu, T. D. Hatchard, A. Bonakdarpour, M. D. Fleischauer, J. R. Dahn, *J. Electrochem. Soc.* **2003**, *150*, 1457.
17 Y. Ohmura, M. Takahashi, M. Suzuki, N. Sakamoto, T. Meguro, *Physica B* **2001**, *308–310*, 257.
18 Y. Ohmura, M. Takahashi, M. Suzuki, A. Emura, N. Sakamoto, T. Meguro, Y. Yamamoto, *Phys. Status Solidi* **2003**, *235*, 111.
19 A. Rantzer, H. Arwin, J. Birch, B. Hjörvarsson, J. W. P. Bakker, K. Järrendahl, *Thin Solid Films* **2001**, *394*, 256.
20 S. Ohara, J. Suzuki, K. Sekine, T. Takamura, *J. Power Sources* **2003**, *119–121*, 591.
21 S. Komaba, T. Itabashi, B. Kaplan, H. Groult, N. Kumagai, *Electrochem. Commun.* **2003**, *5*, 962.
22 H. Momose, H. Honbo, S. Takeuchi, K. Nishimura, T. Horiba, Y. Muranaka, Y. Kozono, H. Miyadera, *J. Power Sources* **1997**, *68*, 208.